Comparison between the Backbone Dynamics of an 11-Amino Acid Peptide Sequence in α-Helical and β-Hairpin Structural Contexts†

Virginia A. Jarymowycz, Ewa Krupinska, and Martin J. Stone*

Department of Chemistry and Interdisciplinary Biochemistry Program, Indiana University, Bloomington, Indiana 47405-0001

Received May 4, 2006; Revised Manuscript Received July 3, 2006

ABSTRACT: To investigate the relationship between backbone motions and the structural environment of a peptide sequence, we have used ^{15}N NMR relaxation data to characterize the backbone motions of the "chameleon-α" (Chm-α) and "chameleon-β" (Chm-β) proteins designed previously by Minor and Kim [Minor, D. L., Jr., and Kim, P. S. (1996) *Nature 380,* 730−734]. These two proteins contain an identical 11-amino acid sequence (dubbed the "chameleon" peptide sequence) in α-helix and β-hairpin conformations, respectively, within the B1 domain of protein G. When placed in an α-helical context, the chameleon peptide shows very limited backbone motions, but some remote regions of the protein are induced to undergo conformational exchange motions, apparently due to modification of packing interactions with the chameleon peptide. In contrast, within a β-hairpin context, the chameleon peptide displays substantial motions on both picosecond and microsecond-to-millisecond time scales, suggesting that it cannot be readily accommodated within the native reverse turn structure. These observations are consistent with the relatively low stability of the Chm-β protein and can be rationalized in terms of native turn-stabilizing interactions that may be disrupted in the Chm-β protein.

Protein dynamics, the internal motions of protein molecules, have the potential to play important roles in controlling protein stability and function. In recent years, there have been significant developments in the experimental observation of protein dynamics using NMR[1] relaxation-based approaches. These new methods have now been applied to numerous proteins and protein complexes (reviewed in refs *1*−*3*) and are steadily improving our understanding of the functional roles of protein dynamics. Considering this progress, we anticipate that future efforts to modify the functions of proteins or to design novel proteins de novo will benefit from strategies that control the protein dynamics as well as the average structure. For this reason, it is important to elucidate the factors that control the motions of backbone and side chain groups in proteins.

One of the critical descriptors of protein dynamics available from NMR relaxation studies is the order parameter (S^2), which characterizes the degree to which rotational motions of a particular group (e.g., N−H bond) are restricted by the surrounding protein matrix. To date, two statistical studies have examined the relationships between order parameters and the structural environments of the relevant groups. These studies have examined trends among backbone amide groups for 20 proteins and side chain methyl groups for eight proteins (*4*, *5*). At the level of primary structure, backbone amide group order parameters were found to correlate weakly with the volume of the side chain in the same amino acid and to a lesser degree with the volumes of neighboring amino acids (*4*), whereas distributions of side chain methyl group order parameters appear to be related to side chain length (*5*). At the level of secondary structure, distributions of backbone order parameters exhibited subtle differences between classes of structural elements (*4*). For example, residues located in helices have higher order parameters (more restricted motions), on average, than those found in β-structures and loops. At the tertiary structure level, backbone order parameters were weakly related to the degree of burial from solvent (*4*).

Several experimental studies have provided information pertinent to the relationships between backbone order parameters and primary or tertiary structure. By varying the amino acid type at a single ("guest") position on the surface of the B1 domain from protein G, we investigated the role of primary sequence in both backbone and side chain dynamics but found no simple correlation between the order parameters and the properties of the guest amino acid (*6*−*8*). The relationship between tertiary packing and backbone dynamics has been probed using core mutants of thioredoxin, the SH3 domain from the Fyn tyrosine kinase, bovine pancreatic trypsin inhibitor, and T4 lysozyme (*9*−*13*). In these systems, the removal of steric constraints generally resulted in increased flexibility on the picosecond time scale and/or the microsecond-to-millisecond time scale. Subsequently, Zhang and Bruschweiler demonstrated that backbone order parameters can be predicted reasonably well from

† This work was supported by a grant awarded to M.J.S. from the National Science Foundation (MCB-0212746).

* To whom correspondence should be addressed: Department of Chemistry, Indiana University, Bloomington, IN 47405-0001. Phone: (812) 855-6779. Fax: (812) 855-8300. E-mail: mastone@indiana.edu.

[1] Abbreviations: Chm-α, chameleon-α; Chm-β, chameleon-β; CD, circular dichroism; η_{xy}, cross-relaxation rate constant; HSQC, heteronuclear single-quantum coherence; NMR, nuclear magnetic resonance; NOE, nuclear Overhauser effect; R_1, longitudinal relaxation rate constant; R_2, transverse relaxation rate constant; R_{ex}, conformational exchange rate; S^2, order parameter; τ_e, internal correlation time; τ_m, rotational correlation time.

10.1021/bi0608919 CCC: $33.50
Published on Web 08/26/2006

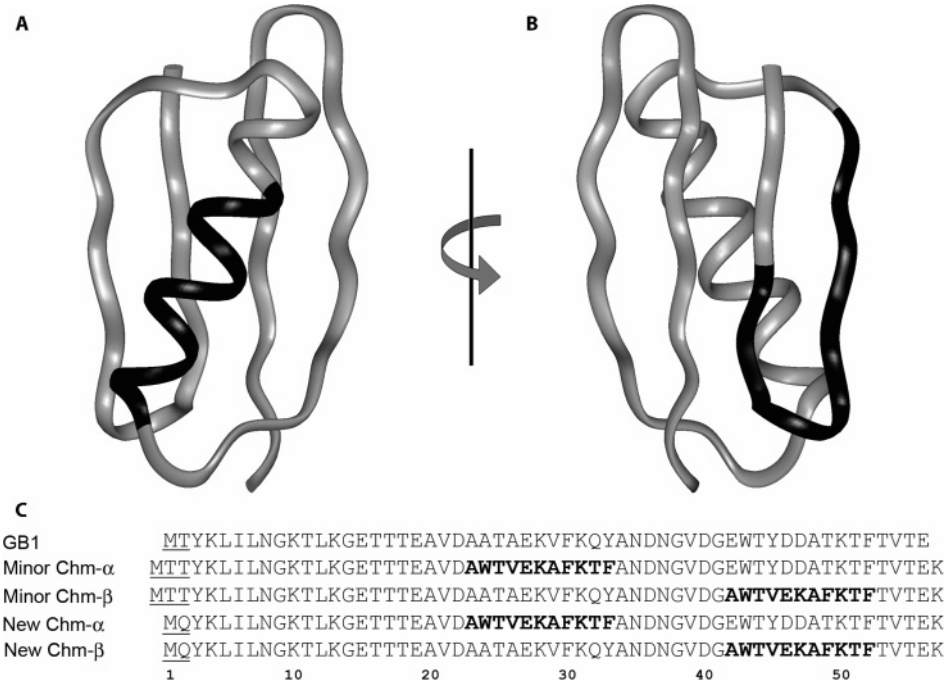

FIGURE 1: Structure of the B1 domain of protein G (PDB entry 3GB1) indicating, in black, the positions of the chameleon peptide sequence in (A) Chm-α (residues 23−33) and (B) Chm-*β* (residues 42−52). Note that the structure in panel B is rotated 180° around the vertical axis relative to the structure in panel A. (C) Sequences of the wild-type B1 domain of protein G which does not include the T2Q mutation, the Chm-α and Chm-*β* constructs designed by Minor and Kim (*15*), or the modified Chm-α and Chm-*β* constructs used in this study. The chameleon peptide sequence is in bold type. Differences in the amino terminus are underlined.

structural coordinates by accounting for the packing interactions of the amide proton and the carbonyl oxygen atom in the same peptide bond (*14*). To date, no studies in which the influence of secondary structure on backbone order parameters has been directly investigated experimentally have been reported.

To gauge the degree to which secondary structure influences internal protein motions, one would ideally need to probe the dynamics of an identical protein sequence in differing secondary, yet identical tertiary, structural environments. Achieving these criteria is impossible because tertiary interactions are dependent on the contributing secondary structural elements. Nevertheless, a comparison of the same peptide sequence in two distinct secondary structure environments can be made using the "chameleon-α" (Chm-α) and "chameleon-*β*" (Chm-*β*) proteins designed by Minor and Kim (*15*). These two proteins contain an identical 11-amino acid sequence (dubbed the "chameleon" peptide sequence) in α-helix and *β*-hairpin conformations, respectively, within the B1 domain of protein G (Figure 1) (*15*). Chm-α and Chm-*β* exhibit reversible thermal unfolding with midpoints of 61.4 and 39.2 °C, respectively (*15*). Although these thermal stabilities are considerably lower than that of the wild-type B1 domain (T_m = 87 °C), NMR experiments produced well-dispersed spectra at 5 °C indicating that the proteins are well-folded. Thus, the chameleon proteins are probably the best available model system for investigating the influence of secondary structural context on protein dynamics.

In this paper, we describe the backbone amide group dynamics of the two chameleon proteins and compare them to each other and to the wild-type B1 domain. We discuss variations in both fast time scale and slow time scale dynamics of the chameleon sequence as a result of structural context and provide a rationale for these changes in terms of the protein structure.

MATERIALS AND METHODS

Sample Preparation. Chm-α and Chm-*β* gene constructs were synthesized on the basis of the chameleon protein sequences (*15*) using recursive PCR and subcloned into a pET11a vector (Novagen, Madison, WI) for *Escherichia coli* expression. The recombinant vectors were transformed into BL21(DE3) *E. coli* cells and grown in LB medium at 37 °C to an optical density (600 nm) of ∼0.6. The temperature was reduced to 25 °C, and isopropyl *β*-D-thiogalactopyranoside (IPTG) was added to a final concentration of 1 mM. After being grown for 4 h at 25 °C, the cells were harvested by centrifugation at 7000 rpm for 10 min. Chm-α cells were resuspended in ∼10 mL of 20 mM Tris-HCl (pH 8) per liter of growth medium, and Chm-*β* cells were resuspended in ∼10 mL of 50 mM Tris-HCl and 150 mM NaCl (pH 7.6) per liter of growth medium. Cells were lysed by sonication. Cell lysate was centrifuged at 15 000 rpm for 30 min, treated with poly(ethyleneimine) to a final concentration of 3%, stirred for 1 h at 4 °C, and centrifuged for 50 min at 15 000 rpm. The supernatant was filtered using a 0.2 *μ*m filter. The Chm-α protein was purified at 25 °C as described for the wild-type B1 domain (*16*). The Chm-*β* protein was purified at 25 °C by IgG affinity chromatography using IgG Sepharose 6 Fast Flow (Amersham Biosciences, Piscataway, NJ) according to the manufacturer's instructions. Eluted Chm-*β* protein was dialyzed into 20 mM Tris-HCl and 300 mM NaCl (pH 8) and further purified by size exclusion chromatography using a HiPrep 16/60 Sephacryl S-100 HR column (Amersham Biosciences). The final purity of the proteins was determined by MALDI-TOF mass spectrometry and SDS−PAGE analysis. Protein concentrations were

determined from the absorbance at 280 nm using extinction coefficients of 13 980 L mol^{-1} cm^{-1} for Chm-α and 8480 L mol^{-1} cm^{-1} for Chm-β, calculated from each protein's amino acid sequence. In a modification to the protocol mentioned above, samples prepared for backbone dynamics experiments were grown in M9 minimal medium containing 6.0 g/L Na_2HPO_4, 3.0 g/L KH_2PO_4, 0.5 g/L NaCl, 1 g/L $^{15}NH_4Cl$, 2 g/L glucose, 2 mM $MgSO_4$, and 0.1 mM $CaCl_2$.

Circular Dichroism Spectroscopy and Thermal Unfolding. The circular dichroism (CD) samples were prepared by dialyzing Chm-α or Chm-β in 50 mM sodium acetate and 150 mM NaCl (pH 5.4). The protein concentrations of the CD samples were 20 μM. CD spectra were acquired on a Jasco J-715 circular dichroism spectropolarimeter. Thermal unfolding was monitored by measuring the ellipticity at 218 nm over a temperature range of 0−90 °C. The temperature was increased from 0 to 76 °C and then decreased to 0 °C in 2 °C increments to assess reversibility. The temperature was increased from 0 to 10 °C in 1 °C increments to obtain a lower baseline for Chm-β and from 72 to 90 °C in 2 °C increments to obtain an upper baseline for both Chm-α and Chm-β. Each data point was collected after a 90 s temperature equilibration time from 16 wavelength scans (217−223 nm). Thermal stability was determined by fitting molar ellipticity measured at 218 nm to the following equation (*17*) using KaleidaGraph (Synergy Software):

$$\theta = \theta_U + (\theta_F - \theta_U)/(1 + e\{(-\Delta H_m/R)(1/T - 1/T_m) + (\Delta C_p/R)[(T_m/T - 1) + \ln(T/T_m)]\})$$

where θ is the molar ellipticity at 218 nm, θ_F and θ_U are linear functions representing the folded and unfolded baselines, respectively, T_m is the melting temperature, ΔH_m is the enthalpy of unfolding at T_m, and ΔC_p is 621 cal mol^{-1} K^{-1} (*18*). Data are presented as the calculated percent folded rather than raw ellipticity values.

NMR Measurements. NMR samples consisted of uniformly ^{15}N-labeled Chm-α or Chm-β in 150 mM NaCl, 50 mM acetic acid-d_4, 0.02% NaN_3, and a H_2O/D_2O mixture (90:10) (pH 5.4). NMR spectra were acquired at 0 °C (at which the solution remains in the liquid state) on a Varian UnityINOVA 500 MHz spectrometer equipped with three radio frequency channels, pulsed field gradients, and a ^1H-detection triple-resonance (HCN) probe. The ^{15}N longitudinal relaxation rate (R_1), ^{15}N transverse relaxation rate (R_2), {^1H}−^{15}N steady-state nuclear Overhauser enhancement (NOE), and ^{15}N transverse cross-relaxation rate constants (η_{xy}) were measured using published two-dimensional $^1H-^{15}N$ HSQC-style pulse sequences (*19*−*21*). The ^1H carrier was placed on the water resonance, and the ^{15}N carrier was placed at 120 ppm. All experiments were acquired with spectral widths of 7000 Hz in the ^1H dimension and 2000 Hz in the ^{15}N dimension. Other experimental parameters were the same as those used in a previous study, except that NOE spectra were recorded in duplicate rather than triplicate (*16*). Backbone amide resonance assignments were made primarily on the basis of published resonance assignments (*15*). However, uncertainties in assignments were addressed using three-dimensional TOCSY-HSQC and NOESY-HSQC spectra, in which the ^1H and ^{15}N carrier frequencies were the same as stated above and the spectral widths were 7000, 6000, and 2000 Hz in the indirect ^1H, direct ^1H_N, and ^{15}N dimensions, respectively (*22*).

Data Analysis. NMR data were processed using FELIX98 (Molecular Simulations, Inc.). All spectra were processed using 3 Hz line broadening in the direct dimension, 90°-shifted sine bell functions in the indirect dimensions, a low-pass filter to suppress solvent signal, and polynomial baseline correction. Relaxation parameters and standard errors were extracted as described previously (*16*). Backbone amide groups with large amplitude internal motions on a picosecond time scale were identified by characteristically low NOE values (NOE < 0.5). Among the remaining backbone amide groups, those with conformational exchange (R_{ex}) on a slow (microsecond to millisecond) time scale were identified by R_2/η_{xy} ratios exceeding the average by one standard deviation (*23*). In each instance, amide groups displaying extremely fast motions or slow conformational exchange were excluded from estimation of each protein's overall correlation time (τ_m) and rotational diffusion tensor. In Chm-α, one residue (Lys-57) was excluded on the basis of a low NOE and five residues (Thr-11, Leu-12, Thr-18, Glu-19, and Gly-41) were excluded on the basis of high R_2/η_{xy} ratios. In Chm-β, two residues (Lys-50 and Lys-57) were excluded on the basis of low NOE values and three residues (Gly-9, Lys-47, and Thr-51) were excluded on the basis of high R_2/η_{xy} ratios. Overall correlation times and diffusion tensors for isotropic, axially symmetric, and fully anisotropic models were calculated from the R_2/R_1 ratios of the remaining residues (34 of 57 backbone amide groups for Chm-α and 42 of 57 backbone amide groups for Chm-β) and the NMR structure coordinates (PDB entry 3GB1) (*24*) using the program quadric_diffusion (A. G. Palmer, III, Columbia University, New York, NY) (*25*). The most appropriate diffusion tensor was selected using *F*-statistical analysis and from a comparison of χ^2 goodness-of-fit parameters. Following estimation of the rotational diffusion tensors, relaxation data were fit to five versions of the Lipari−Szabo model-free formalism (*26*−*30*) commonly termed "models" 1−5 using Modelfree (A. G. Palmer, III) which optimizes one or more of each amide group's internal motional parameters (S^2,τ_e, and R_{ex}). The fitted parameters for the five models are as follows: model 1, order parameter (S^2); model 2, S^2 and internal correlation time (τ_e); model 3, S^2 and exchange broadening contribution to transverse relaxation (R_{ex}); model 4, S^2, τ_e, and R_{ex}; and model 5, order parameters for two time scales (S_f^2 and S_s^2) and τ_e for the slower time scale. Fitting procedures and model selection were performed with ModelFree as previously described (*31*). After selection of the most appropriate model for each residue, ModelFree was used to simultaneously optimize the rotational diffusion tensor and all dynamics parameters. Uncertainties in the dynamics parameters were obtained from 500 Monte Carlo simulations carried out by ModelFree.

RESULTS

Expression Systems. The sequences of the chameleon proteins used in this study are shown in Figure 1. Note, in particular, that the chameleon peptide sequence spans residues 23−33 (the α-helix) in Chm-α and residues 42−52 (the β3−β4 hairpin turn) in Chm-β. Genes encoding the published Chm-α and Chm-β protein sequences (*15*) were overexpressed and purified from *E. coli*. Expression at 25 °C yielded proteins that were folded at 4 °C, as assessed by

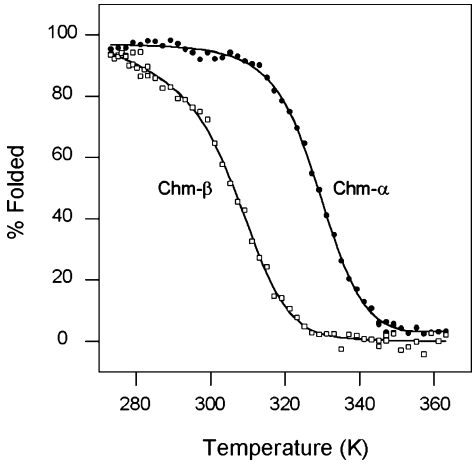

FIGURE 2: Thermal unfolding curves for Chm-α (●) and Chm-β (□) as measured by CD. The percent folded for Chm-α and Chm-β was calculated from the molar ellipticity (θ) measured at 218 nm, and curve fits (—) were obtained as described in Materials and Methods.

CD spectroscopy. Despite the previous finding that insertion of a threonine residue between Met-1 and Thr-2 produced an N-terminally processed protein beginning with the inserted threonine residue (*17*), mass spectrometry analysis of the purified proteins indicated a heterogeneous population of each chameleon protein, with and without an N-terminal methionine. Consequently, genes encoding both chameleon proteins were modified to remove the inserted threonine and to replace the wild-type Thr-2 residue with Gln; the T2Q mutation has previously been found to prevent processing of the N-terminal methionine (*32*). Overexpression and purification of these new chameleon constructs at 25 °C resulted in folded, homogeneous Chm-α and Chm-β proteins, in which the N-terminal methionine residues had not been processed. The "wild-type" B1 domain discussed below includes this T2Q modification (*32*).

Folding Stability. The folding stability of Chm-α and Chm-β was assessed by monitoring the ellipticity at 218 nm as a function of temperature using CD spectroscopy. As previously observed, both proteins display cooperative reversible thermal unfolding (Figure 2) (*15*). From the unfolding data, Chm-α was found to have a melting temperature of 56.2 ± 0.4 °C and an enthalpy of unfolding at the melting temperature (ΔH_m) of 34.7 ± 1.5 kcal/mol. Considering the N-terminal modifications discussed above, these values compare reasonably well with those determined previously by Minor and Kim (T_m = 61.4 °C, and ΔH_m = 41.5 kcal/mol) (*15*). Chm-β was less thermally stable, with a T_m of 35.7 ± 1.0 °C and a ΔH_m of 28.8 ± 1.3 kcal/mol, again in adequate agreement with the previous report (T_m = 39.2 °C, and ΔH_m = 27.7 kcal/mol) (*15*). The fitted thermodynamics values were used to determine the stability profile of each chameleon protein. On the basis of these profiles, we chose to take NMR relaxation measurements at 0 °C. At this temperature, both proteins are expected to exhibit maximal stability, with 99.4% of Chm-α in the folded state and 97.5% of Chm-β in the folded state. Under these conditions, the relaxation rates are dominated by the folded state of each protein, and differences in the derived dynamical parameters can be confidently ascribed to differences between the dynamics of the folded structures.

Initial Relaxation Parameters. Relaxation parameters (R_1, R_2, NOE, and η_{xy}) were determined for 40 of 57 backbone amide groups in a 0.9 mM sample of Chm-α and 47 of 57 backbone amide groups in a 0.9 mM sample of Chm-β. Relaxation parameters were not determined for a number of amide groups in both proteins due to partial or complete spectral overlap or ambiguous assignments. The R_1, R_2, NOE, R_2/R_1, and R_2/η_{xy} values for both proteins are plotted in Figure 3 and listed in the Supporting Information. The average relaxation values for each protein are given in Table 1. The chameleon proteins display similar patterns of longitudinal relaxation (R_1) across the protein sequence, although the values are slightly reduced for Chm-α with an average R_1 value (±standard deviation) of 1.72 ± 0.10 compared with a value of 1.82 ± 0.12 for Chm-β. In contrast, differences in transverse relaxation (R_2) between the two proteins are more dramatic, with average values of 12.72 ± 1.92 for Chm-α and 9.46 ± 2.44 for Chm-β. Additionally, Chm-α displays higher-than-average R_2 values for multiple amide groups in the $\beta1-\beta2$ turn and $\beta2$ strand (residues 9, 11, 18, and 19) preceding the Chm-α sequence (residues 23−33), whereas Chm-β displays nonuniform R_2 values for a number of amides (residues 47, 50, and 51) within the Chm-β sequence (residues 42−52). These differences in patterns of transverse relaxation manifest in plots of R_2/R_1 and R_2/η_{xy} values for both proteins as well (Figure 3D,F). In particular, residues Thr-11, Leu-12, Thr-18, Glu-19, and Gly-41 of Chm-α and residues Gly-9, Lys-47, Lys-50, and Thr-51 of Chm-β were all found to have R_2/η_{xy} values greater than one standard deviation above the average, suggesting conformational exchange on a slow time scale. Patterns of NOE values for both proteins are relatively uniform, with slightly elevated NOE values for Chm-α (average NOE = 0.72 ± 0.10) compared with those of Chm-β (average NOE = 0.66 ± 0.19). Exceptions include C-terminal residue Lys-57 in both proteins, which display NOE values between 0.3 and 0.35, as well as residue Lys-50 in Chm-β which displays an NOE value of −0.48.

Initial Diffusion Tensor Calculations. The rotational diffusion tensor for each chameleon protein was calculated from R_2/R_1 ratios of amide groups not exhibiting large amplitude motions on a fast time scale or conformational exchange on a slow time scale (see Materials and Methods). For both proteins, we found a statistically significant improvement in the fit of the axially symmetric diffusion model relative to the isotropic model ($F_{exp} > F_{0.95}$), whereas there was no significant improvement in the fit for the fully anisotropic model compared with the axially symmetric model ($F_{exp} < F_{0.95}$). A comparison of χ^2 goodness-of-fit parameters indicated a prolate axially symmetric diffusion tensor fit the data better than an oblate axially symmetric model. The four parameters (τ_m, $D_\perp/D_{||}$, θ, and ϕ) defining the axial prolate diffusion tensor for each protein are listed in Table 2. Although the dimensions and orientation of the diffusion tensors for the two chameleon proteins are similar, the overall correlation times (τ_m) are radically different. Chm-β was found to have a τ_m value of ~7.5 ns, which is similar to that of the wild-type protein at 0 °C (τ_m = 7.0 ns) (*16*). However, the rotational correlation time of Chm-α was much slower (~9.5 ns), suggesting self-association of this protein.

Analysis of Aggregation of Chm-α. The observation of reduced R_1 values and elevated R_2 values for Chm-α

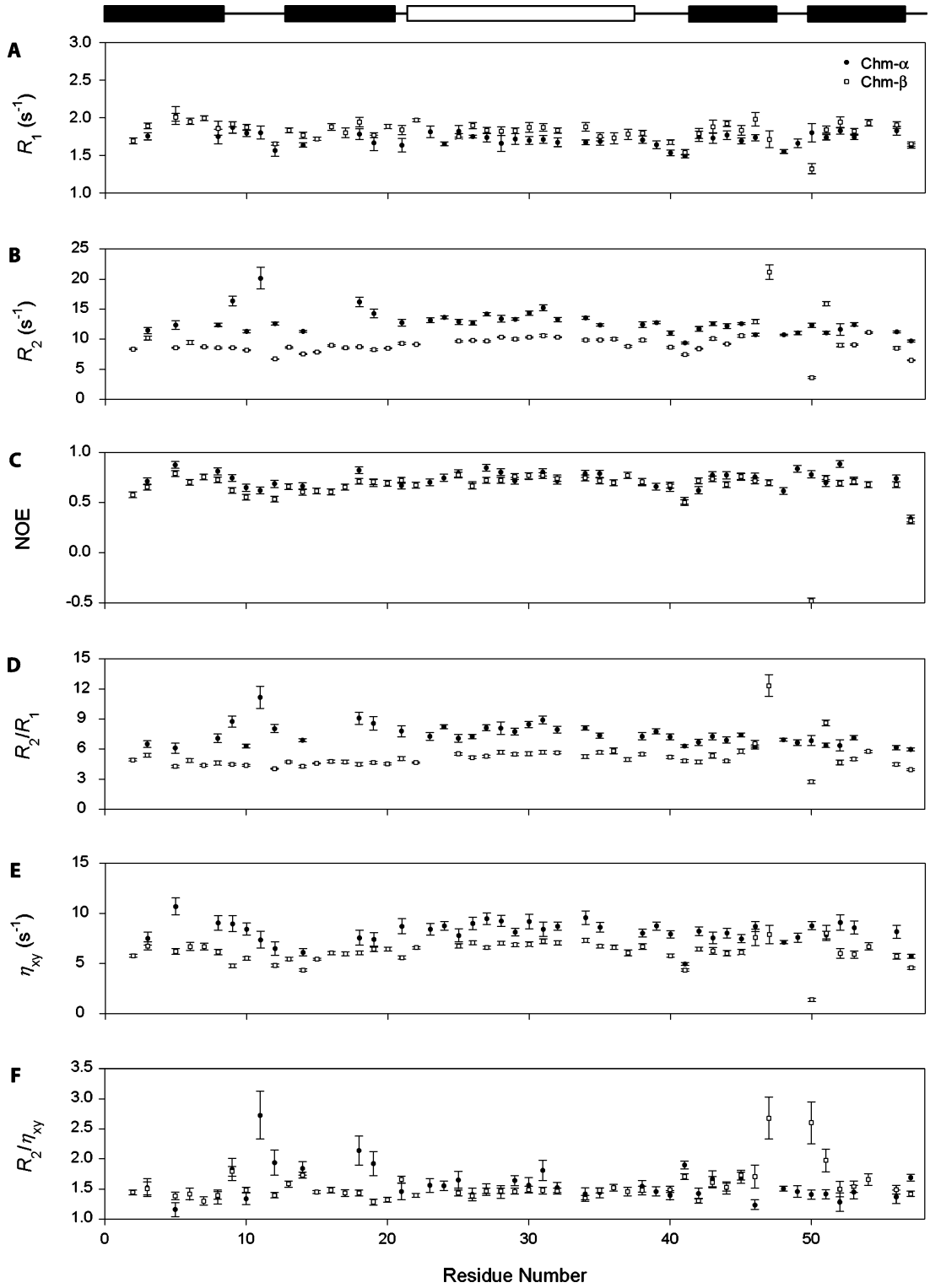

FIGURE 3: Plots of relaxation parameters (A) R_1, (B) R_2, (C) NOE, (D) R_2/R_1, (E) η_{xy}, and (F) R_2/η_{xy} for 0.90 mM Chm-α (●) and 0.90 mM Chm-β (□) as a function of residue number. The positions of the β-strands and the α-helix are indicated schematically at the top with black rectangles and a white rectangle, respectively.

compared with those of Chm-β and the wild-type B1 domain, along with a significantly slower rotational correlation time, suggests that Chm-α undergoes self-association at a concentration of 0.9 mM. To determine whether aggregation was occurring, the R_1, R_2, and NOE experiments were repeated for Chm-α at three protein concentrations (1.08, 0.56, and 0.28 mM) and diffusion tensors were calculated for the protein at each concentration (Table 3). The τ_m values decreased monotonically (from 10.1 to 8.8 ns and from 8.8 to 7.9 ns) with a decrease in protein concentration. The τ_m value of ~7.9 ns for the most dilute sample is only slightly higher than that for the 0.9 mM sample of Chm-β (7.5 ns), indicating that 4-fold dilution eliminates a substantial fraction of the self-association. We can estimate the proportion of Chm-α in the monomeric form at the lowest concentration by making the simplifying assumptions that (1) τ_m for the Chm-α monomer is the same as τ_m for Chm-β, (2) the self-associated species is a dimer, (3) the apparent τ_m for the

Table 1: Average Relaxation Parameters[a]

	2.7 mM wild-type B1 domain (*16*)	0.90 mM Chm-α	0.28 mM Chm-α	0.90 mM Chm-*β*
R_1 (s^{-1})	1.90 ± 0.11	1.72 ± 0.10	1.79 ± 0.11	1.82 ± 0.12
R_2 (s^{-1})	8.40 ± 0.76	12.72 ± 1.92	10.26 ± 2.47	9.46 ± 2.44
NOE	0.75 ± 0.05	0.72 ± 0.10	0.73 ± 0.10	0.66 ± 0.19
R_2/R_1	4.43 ± 0.41	7.41 ± 1.03	5.77 ± 1.48	5.18 ± 1.35
η_{xy}	5.68 ± 0.64	8.22 ± 1.08	*b*	6.16 ± 1.10
R_2/η_{xy}	1.49 ± 0.11	1.58 ± 0.28	*b*	1.55 ± 0.27

[a] Relaxation data reported as the average ± the standard deviation. [b] Not determined.

Table 2: Rotational Diffusion Parameters[a]

	2.7 mM wild-type B1 domain (*16*)	0.90 mM Chm-α	0.28 mM Chm-α	0.90 mM Chm-*β*
no. of residues	55	34	34	42
τ_m (ns)	7.00	9.49 ± 0.09	7.94 ± 0.12	7.49 ± 0.21
$D_{\|\|}/D_\perp$	1.34 ± 0.04	1.26 ± 0.05	1.29 ± 0.08	1.28 ± 0.05
θ (deg)	85 ± 3	79.5 ± 6.1	88.8 ± 17.3	75.9 ± 30.2
ϕ (deg)	182 ± 6	181.5 ± 6.8	4.4 ± 7.2	175.2 ± 13.4

[a] The parameters for all proteins were determined using an axially symmetric prolate diffusion tensor where τ_m is the overall correlation time defined as $(2D_{||} + 4D_\perp)^{-1}$, where $D_\perp/D_{||}$ is the ratio of the diffusion rate constants around unique and perpendicular axes of the diffusion tensor, and θ and ϕ are the Euler angles defining the position of the unique axis, as reported by the program quadric_diffusion.

Table 3: Concentration Dependence of Rotational Diffusion Parameters for Chm-α[a]

	1.08 mM Chm-α	0.56 mM Chm-α	0.28 mM Chm-α
no. of residues	34	34	34
τ_m (ns)	10.11 ± 0.12	8.76 ± 0.11	7.94 ± 0.12
$D_{\|\|}/D_\perp$	1.28 ± 0.06	1.31 ± 0.08	1.29 ± 0.08
θ (deg)	87.6 ± 9.6	92.0 ± 10.2	88.8 ± 17.3
ϕ (deg)	10.2 ± 0.9	−1.8 ± 7.4	4.4 ± 7.2

[a] The parameters are as defined in the footnote of Table 2.

Chm-α dimer scales with the τ_m for the Chm-α monomer by a factor of 2−3.165 [2 corresponds to the Stokes−Einstein scaling for isotropic diffusion of spherical particles, whereas 3.165 corresponds to the relationship derived by Schurr et al. for the case of an elongated dimer formed from isotropic monomers (*33*)], and (4) the observed τ_m value is a population-weighted average of monomer and dimer values. In this case, we calculate that Chm-α is 94−97% monomeric in the 0.28 mM sample. The assumption of higher-order oligomeric species (trimer, tetramer, etc.), with correspondingly higher correlation times, would yield the conclusion that an even higher proportion of Chm-α is monomeric. Consequently, we conclude that the 0.28 mM Chm-α sample contained predominantly monomeric species. It remains possible that the small fraction of aggregate could influence the magnitudes of the calculated internal dynamical parameters (*33*). However, this effect is unlikely to influence the variation of dynamical parameters across the protein sequence to a noticeable degree (*33*). Consequently, it is valid to compare these variations for the 0.28 mM sample of Chm-α and the 0.90 mM sample of Chm-*β*. The dynamics data presented and discussed below are for these two samples.

Relaxation and Dynamics Parameters for Chm-β and Diluted Chm-α. The R_1, R_2, NOE, and R_2/R_1 values for the 0.28 mM Chm-α sample and the 0.9 mM Chm-*β* sample are plotted in Figure 4 and listed in the Supporting Information. The average relaxation values for each sample are given in Table 1, along with the values for the more concentrated sample of Chm-α. The variations of relaxation parameters across the protein sequence are very similar for the diluted sample of Chm-α to those discussed above for the more concentrated sample. However, consistent with the decreased level of aggregation, the more dilute sample displays an increased average value of R_1 and decreased average values of R_2 and R_2/R_1, closer to those observed for the Chm-*β* protein (Table 1). Interestingly, the average NOE value remains slightly elevated for the low-concentration Chm-α sample relative to the value for Chm-*β* (Table 1).

Dynamics parameters for Chm-α and Chm-*β* were obtained by fitting relaxation data to the Lipari−Szabo model-free formalism (*26*−*30*). Model-free analysis yields three basic dynamics parameters describing the internal motions of each backbone amide bond vector: the generalized order parameter S^2, which is a measure of the degree of spatial restriction of the vector's motion (completely restricted motions have an S^2 of 1 and completely unrestricted motions an S^2 of 0), the effective correlation time τ_e, which is a measure of the rate of vector motion, and R_{ex}, which is a measure of conformational exchange on a slow time scale. These parameters are called "model-independent" because the model-free formalism itself does not invoke a specific motional model to describe the internal bond vector motion. However, relaxation data for each vector are fit to one of five versions of the model-free formalism commonly termed models 1−5 (Materials and Methods).

Model-free analyses were performed for Chm-α (data for the 0.28 mM sample) and Chm-*β*, each using the rotational diffusion tensor determined for the same protein. As a control, additional model-free calculations were performed for relaxation data of each protein using the diffusion tensor of the other protein. Model-free parameters determined using the latter method were not significantly different from those determined using each protein's own diffusion tensor, indicating that the differences between Chm-α and Chm-*β* dynamics parameters discussed below do not arise from the different diffusion tensors of the two proteins.

Among the 39 and 46 backbone amide groups included in model-free analyses for Chm-α and Chm-*β*, respectively, relaxation data for the majority of amides could be fit to model 1 (25 and 14 groups, respectively) or model 2 (8 and 23 groups, respectively). Addition of a slow conformational exchange term (R_{ex}, model 4) was required for 5 residues in Chm-α and 6 residues in Chm-*β*, and the remaining residues (1 in Chm-α and 3 in Chm-*β*) were fit using model 5, which describes motions on two distinct time scales faster than molecular tumbling.

In the case of Chm-α, an R_{ex} term was required to adequately fit relaxation data to the model-free formalism for residues Gly-9, Thr-11, Leu-12, Thr-18, and Glu-19, whereas in the case of Chm-*β*, residues Tyr-3, Val-45, Glu-46, Lys-47, Thr-51, and Thr-54 required an R_{ex} term. Relaxation data for residue Gly-41 in Chm-α and residues Leu-12, Asp-22, and Lys-50 in Chm-*β* were fit to model 5,

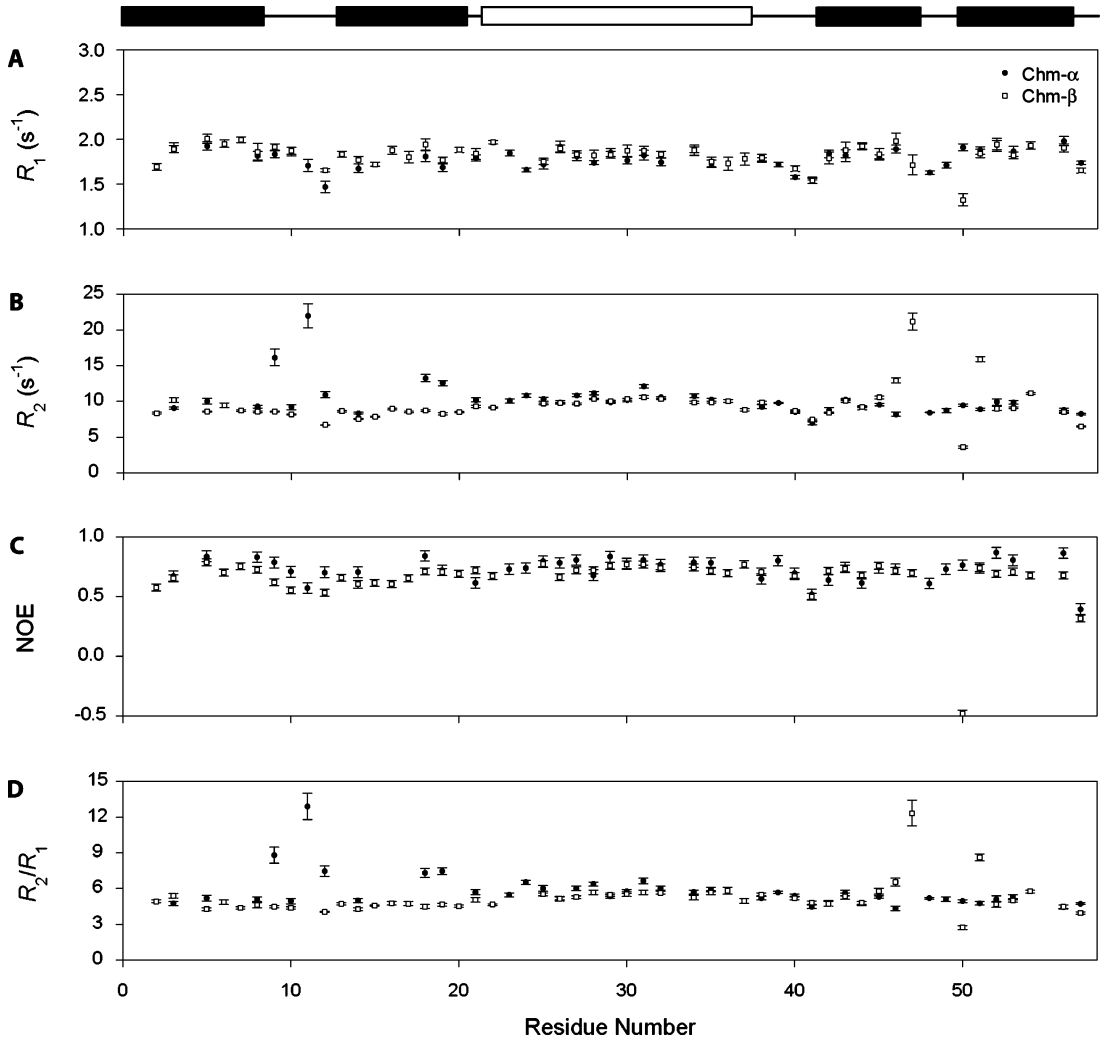

FIGURE 4: Plots of relaxation parameters (A) R_1, (B) R_2, (C) NOE, and (D) R_2/R_1 for 0.28 mM Chm-α (●) and 0.90 mM Chm-β (□) as a function of residue number. The positions of the β-strands and the α-helix are indicated schematically at the top with black rectangles and a white rectangle, respectively.

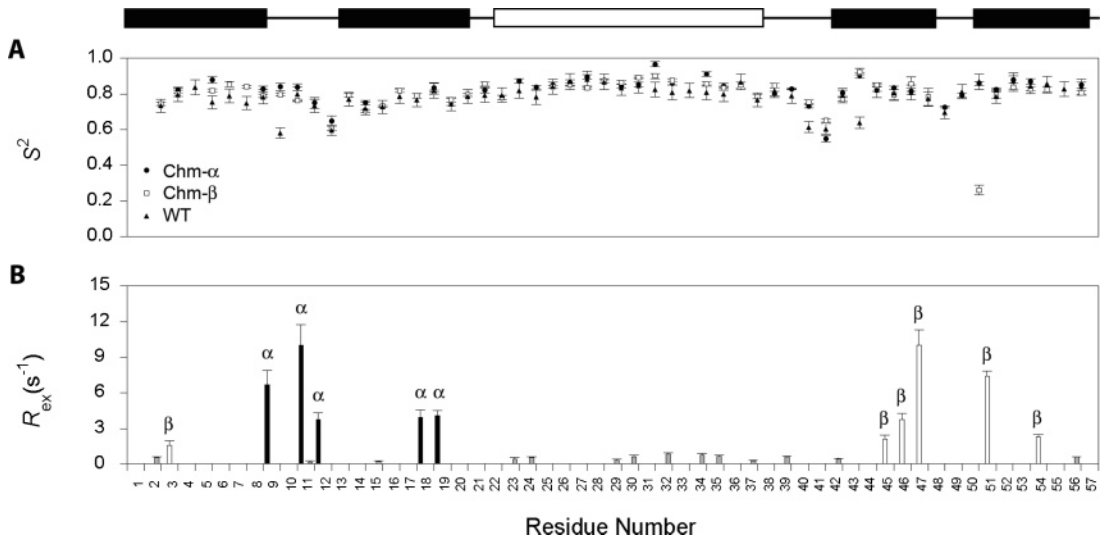

FIGURE 5: Plots of dynamics parameters (A) S^2 and (B) R_{ex} for 0.28 mM Chm-α (● and black bars labeled α), 0.90 mM Chm-β (□ and white bars labeled β), and the wild-type B1 domain (▲ and gray bars) as a function of residue number. The positions of the β-strands and the α-helix are indicated schematically at the top with black rectangles and a white rectangle, respectively.

thus suggesting bond vector motions on slow and fast time scales.

The S^2 and R_{ex} values for the 0.28 mM Chm-α sample and the 0.90 mM Chm-β sample are plotted in Figure 5, along with those of the wild-type protein, and are listed in the Supporting Information. The average dynamics parameters for each protein are given in Table 4. The average S^2 value of Chm-α is slightly higher than those of the other

Table 4: Average Dynamics Parameters[a]

	2.7 mM wild-type B1 domain (*16*)	0.28 mM Chm-α	0.90 mM Chm-*β*
S^2	0.784 ± 0.070	0.824 ± 0.073	0.798 ± 0.100
τ_e (ps)	947 ± 598	138 ± 334	136 ± 301
R_{ex} (s^{-1})	0.52 ± 0.20	5.71 ± 2.68	4.53 ± 3.41

[a] Dynamics data reported as the average ± the standard deviation.

two proteins, possibly reflecting the low level of aggregation remaining in the Chm-α sample (vide supra). Variations of dynamical parameters across the protein sequences and between the Chm-α, Chm-*β*, and wild-type proteins are discussed below.

DISCUSSION

We have reported here backbone dynamical data for two modified forms of the protein G B1 domain (Chm-α and Chm-*β*), each containing the same 11-amino acid peptide sequence substituted into a different region of the structure (α-helix and *β*-hairpin, respectively). Using the data for these two proteins, along with the data previously obtained for the wild-type B1 domain under the same conditions (*16*), we can make comparisons between the motions of a single peptide sequence in two different structural environments and between different peptide sequences in the same region of the structure.

Variations in Fast Time Scale Dynamics across the Protein Sequence. Figure 5 shows the order parameters for each NH group in Chm-α, Chm-*β*, and the wild type B1 domain, representing the degree of restriction of picosecond time scale dynamics at each backbone position in each protein. Despite the substantial stability differences and the substitution of the long chameleon peptide sequence, the distributions of order parameters across the sequence are remarkably similar for the three proteins. In particular, although the order parameters are fairly uniform across the majority of residues, there are distinct regions of increased backbone flexibility in the *β*1−*β*2 turn and α−*β*3 loop. These results suggest that patterns of fast time scale dynamics in these three proteins are substantially determined by the protein fold, with the motions of the backbone being limited by secondary and tertiary packing interactions.

Variations in Fast Time Scale Dynamics as a Result of the Structural Environment. The order parameters within the chameleon sequences of Chm-α and Chm-*β* are compared in Figure 6A. It is important to emphasize that the amino acids in these sequences are identical so any differences in their order parameters can be attributed to differences between their secondary structural contexts and/or tertiary interactions. The only amino acid that displays such a difference is the ninth residue of the chameleon peptide (Lys-31 in Chm-α and Lys-50 in Chm-*β*), whose backbone amide group is dramatically more flexible in the Chm-*β* context (S^2 values of 0.97 ± 0.02 and 0.26 ± 0.03 in Chm-α and Chm-*β*, respectively). This dramatic difference in flexibility is direct experimental evidence that structural environment can indeed have a significant effect on the fast time scale dynamics of a folded amino acid sequence. This observation is consistent with the conclusions of previous statistical analyses, which indicate that both secondary structure and tertiary packing can influence protein backbone dynamics (*4*, *5*).

It is informative to compare the backbone dynamics of the chameleon sequences and the dynamics of the corresponding sequences in the wild-type B1 domain (Figure 6B,C). In the case of Chm-α, order parameters of chameleon sequence residues are nearly identical to those of residues located within the α-helix of the wild-type protein (Figure 6B). The absence of an accompanying change in dynamics with the change in sequence illustrates that the chameleon peptide sequence can be readily accommodated within the α-helical conformation of the wild-type B1 domain, presumably forming the same backbone hydrogen bonds. In this regard, our data provide additional evidence of the success of the original chameleon sequence design and help to explain the fairly high stability of the Chm-α protein.

The comparison between chameleon sequence residues in Chm-*β* and the corresponding residues in the *β*3−*β*4 turn of the wild-type B1 domain (Figure 6C) highlights a significant difference in order parameters at the above-mentioned chameleon position 9 or residue 50 in the B1 domain sequence. Interestingly, residue 50 is a lysine in both Chm-*β* and the wild-type B1 domain, suggesting that the dynamical difference at this position results from differences in the interactions of neighboring residues, as discussed in detail below. In contrast to the success of the design for the Chm-α protein, these results indicate that the chameleon peptide was not optimally accommodated in the *β*-hairpin context, consistent with the substantial destabilization of Chm-*β* compared with the wild-type B1 domain (*15*).

Variations in Slow Time Scale Conformational Exchange across the Protein Sequence. In contrast to the similar patterns of order parameters observed for Chm-α, Chm-*β*, and the wild type B1 domain, the three proteins display considerably different patterns of conformational exchange (Figure 5). The wild-type protein exhibits negligible dynamics on this time scale with an average R_{ex} term for the 14 relevant residues of <1 s^{-1} (*16*), whereas the average (±standard deviation) R_{ex} values for Chm-α and Chm-*β* are 5.7 ± 2.7 ($n = 5$) and 4.5 ± 3.4 s^{-1} ($n = 6$), respectively.

For the Chm-α protein, none of the residues within the chameleon peptide region displays conformational exchange, consistent with the above conclusion that the chameleon peptide is well-accommodated within the α-helical conformation of the B1 domain. Surprisingly, the five amide groups displaying exchange broadening in Chm-α are all located 5−13 Å from chameleon peptide residues, either in the *β*1−*β*2 turn (Gly-9, Thr-11, and Leu-12) or at the end of the *β*2 strand, which precedes the chameleon sequence (Thr-18 and Glu-19). The conformational exchange of Thr-18 and Glu-19 could potentially result from modified packing interactions between the side chain of Thr-18 and the side chain of residue 29, which is mutated from a valine in the wild-type B1 domain to an alanine in Chm-α. The mechanism by which substitution of the α-helical sequence causes dynamical changes in the *β*1−*β*2 turn is less apparent. One possibility is that this effect is propagated via a network of side chain packing interactions from chameleon sequence residue 33 (Tyr in the wild-type B1 domain and Phe in Chm-α) through residues Leu-7 and Asn-37 to residues Gly-9 and Leu-12 in the *β*1−*β*2 turn; no dynamics data are available for Leu-7 and Asn-37 due to spectral overlap.

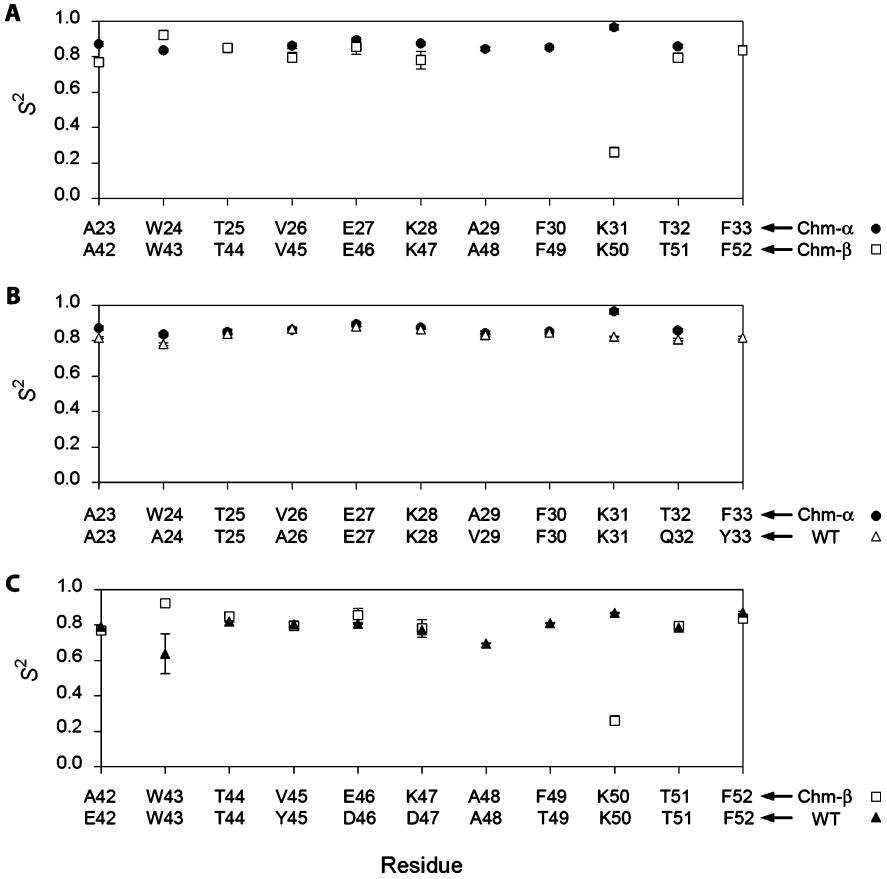

FIGURE 6: Comparison of S^2 values between (A) chameleon sequence residues of 0.28 mM Chm-α (●) and 0.90 mM Chm-β (□), (B) chameleon sequence residues of 0.28 mM Chm-α (●) and α-helical residues 23−33 in the wild-type B1 domain (△), and (C) chameleon sequence residues of 0.90 mM Chm-β (□) and β-hairpin residues 42−52 of the wild-type B1 domain (▲) as a function of chameleon sequence position. If not visible, error bars are hidden by data points.

In Chm-β, five of the six residues with exchange broadening (Val-45, Glu-46, Lys-47, Thr-51, and Thr-54) are located within or sequentially adjacent to the chameleon sequence (residues 42−52). Four of the chameleon sequence residues exhibiting slow conformational exchange are located in the β3−β4 reverse turn. The possible structural basis of dynamical changes in this turn is discussed in detail below. The increased flexibility of the fifth residue, Thr-54 (located in strand β4) could result from altered interactions with the cross-strand residue (Glu-42 in the wild-type B1 domain and Ala-42 in Chm-β). The sixth residue exhibiting slow conformational exchange (Tyr-3) is not located in the chameleon peptide but packs against chameleon residue Lys-50. Together, these observations reinforce the conclusion from the fast time scale dynamics data, indicating that the chameleon peptide does not assume a unique conformation comparable to the β-hairpin of the wild-type protein.

Structural Rationale for the Changes in Reverse Turn Dynamics. The increased flexibility of the β3−β4 turn in Chm-β on both the picosecond and microsecond-to-millisecond time scales can be rationalized by considering the structure of this turn in the wild-type protein (*34*) and the amino acid mutations introduced into Chm-β (*15*); these are illustrated in Figure 7. Whereas the majority of reverse turns consist of four residues, the β3−β4 turn is formed by six residues (Asp-46, Asp-47, Ala-48, Thr-49, Lys-50, and Thr-51), which interact to form a total of five turn-stabilizing hydrogen bonds. In particular, the backbone amide group of Lys-50, which exhibits increased picosecond time scale flexibility in Chm-β, and the amide group of the preceding residue (Thr-49) are both hydrogen-bonded to the backbone carbonyl group of Asp-46 (two orange dashed arrows at the right in Figure 7). In turn, the side chain carboxyl group of Asp-46 is hydrogen-bonded to the backbone amide of Ala-48 (yellow dashed arrow at the left in Figure 7).

In Chm-β, Asp-46 is mutated to Glu and Thr-49 to Phe. The effect of the Asp-46 → Glu mutation can be understood with reference to the published β-turn positional potentials of the amino acids determined from databases of β-turns containing four residues (*35*−*37*). There is a strong preference for residues such as asparagine, aspartic acid, cysteine, and serine at the first position of specific classes of β-turns due to the fact that the atoms at the γ- or δ-positions of their side chains can act as hydrogen bond acceptors and thus form stabilizing hydrogen bonds with the amide nitrogen of the third residue in the turn (*36*, *37*). This is directly analogous to the hydrogen bond between the side chain δ-oxygen of Asp-46 and the backbone amide of Ala-48 in the wild-type B1 domain. Although the side chain of glutamic acid is also capable of acting as a hydrogen bond acceptor, the turn potential of a glutamic acid at turn position 1 is much lower than that of aspartic acid, suggesting that the added chain length of a glutamic acid side chain may prevent formation of the stabilizing hydrogen bond to turn residue 3. Therefore, we propose that the Asp-46 → Glu mutation in Chm-β leads to disruption of the hydrogen bond between residues 46 and 48, the reduced stability of the turn, and the increased flexibility on the microsecond-to-millisecond time

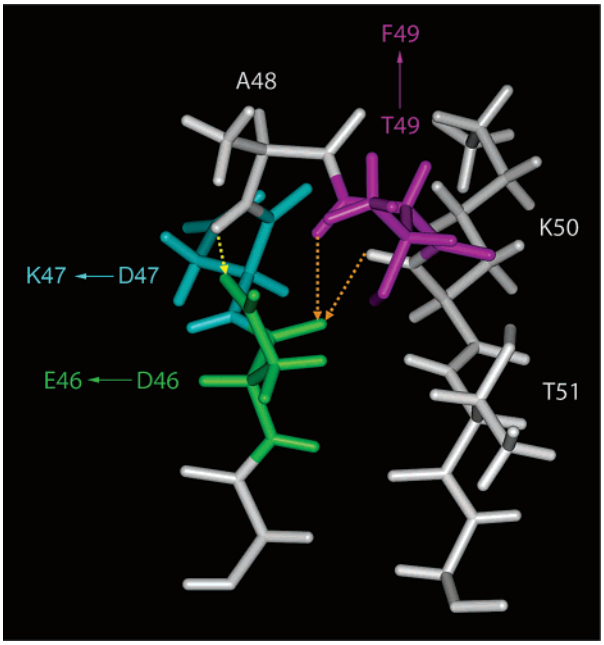

FIGURE 7: Structure of the $\beta3-\beta4$ turn region of the B1 domain of protein G (PDB entry 3GB1). The backbones of residues 45−52 and the side chains of turn residues 46−51 are displayed in stick representation. Residues 46, 47, and 49, which have been mutated in the $\beta3-\beta4$ turn of Chm-β, are colored green, cyan, and magenta, respectively, and the mutations are denoted with solid arrows. Hydrogen bonds between the backbone amide groups of residues 49 and 50 and the backbone carbonyl of residue 46 are indicated by two orange dashed arrows. A hydrogen bond between the backbone amide of residue 48 and the side chain carboxyl of residue 46 is indicated by a yellow dashed arrow.

scale. The effect of this mutation on the fast time scale dynamics is less obvious because relaxation data were not available for residue 48 or 49 of Chm-β. However, it is possible that the disruption of this hydrogen bond allows an increased level of motion of residue 48 that is propagated through the backbone to residues 49 and 50.

A second mutation that could have disrupted the structure of the $\beta3-\beta4$ turn is the Thr-49 → Phe mutation. There is a general preference for hydrophilic rather than hydrophobic residues in turns due to the fact that turns are frequently solvent-exposed. In a study of the conformational preference of amino acids in globular proteins, hydrophobic residues such as alanine, histidine, isoleucine, leucine, methionine, phenylalanine, and valine were classified as "turn-breaking" residues in reverse turns (*35*). Similarly, residues determined to have the lowest overall turn potential in β-turns were also, by and large, hydrophobic (*36*). The replacement of Thr-49 with Phe in Chm-β therefore causes a substantial decrease in the turn potential at that position. One can imagine that the phenylalanine side chain will have a tendency to rotate away from solvent (downward in Figure 7) and that such rotation will be less constrained in Chm-β due to the loss of the hydrogen bond involving the backbone of Ala-48. If such a rotation occurs, it could in turn disrupt the hydrogen bonds from the amide groups of residues 49 and 50 to the backbone carbonyl of residue 46, thus providing an additional possible explanation for the observed flexibility increases on both fast and slow time scales.

Concluding Remarks. We have described herein the backbone flexibility of a peptide sequence when it is placed in each of two distinct structural environments. The results indicate that the mobility of this peptide is substantially dependent on its location within the protein structure rather than on its primary amino acid sequence. Incorporation of the chameleon peptide into an α-helical environment results in restricted backbone motions throughout the peptide sequence. In contrast, incorporation into a β-hairpin environment allows extensive motion on both fast and slow time scales, suggesting that the chameleon sequence does not adopt a unique "nativelike" conformation. The latter dynamics may be related to the relatively low stability of the Chm-β protein. Thus, the data suggest that the optimal stability of the B1 domain requires formation of enthalpically favorable interactions in the $\beta3-\beta4$ turn that are partially offset by a reduction in backbone entropy.

ACKNOWLEDGMENT

We thank Drs. Douglas E. Brown and John W. Tomaszewski (Indiana University NMR Facility), Dr. Todd Stone (Indiana University Physical Biochemistry Instrumentation Facility), and Dr. Daniel L. Minor (University of California, San Francisco, CA) for helpful discussions and Drs. Lewis Kay (University of Toronto, Toronto, ON) and Mark Rance (University of Cincinnati, Cincinnati, OH) for providing pulse programs.

SUPPORTING INFORMATION AVAILABLE

Three tables listing the relaxation data for the original 0.90 mM samples of Chm-α and Chm-β and the 0.28 mM samples of Chm-α and two tables listing the model-free dynamics parameters for the 0.28 mM sample of Chm-α and the original sample of Chm-β. This material is available free of charge via the Internet at http://pubs.acs.org.

REFERENCES

1. Palmer, A. G., III (2004) NMR characterization of the dynamics of biomacromolecules, *Chem. Rev. 104*, 3623−3640.
2. Jarymowycz, V. A., and Stone, M. J. (2006) Fast time scale dynamics of protein backbones: NMR relaxation methods, applications, and functional consequences, *Chem. Rev. 106*, 1624−1671.
3. Igumenova, T. I., Frederick, K. K., and Wand, A. J. (2006) Characterization of the fast dynamics of protein amino acid side chains using NMR relaxation in solution, *Chem. Rev. 106*, 1672−1699.
4. Goodman, J. L., Pagel, M. D., and Stone, M. J. (2000) Relationships between protein structure and dynamics from a database of NMR-derived backbone order parameters, *J. Mol. Biol. 295*, 963−978.
5. Mittermaier, A., Kay, L. E., and Forman-Kay, J. D. (1999) Analysis of deuterium relaxation-derived methyl axis order parameters and correlation with local structure, *J. Biomol. NMR 13*, 181−185.
6. Stone, M. J., Gupta, S., Snyder, N., and Regan, L. (2001) Comparison of protein backbone entropy and β-sheet stability: NMR-derived dynamics of protein G B1 domain mutants, *J. Am. Chem. Soc. 123*, 185−186.
7. Mayer, K. L., Earley, M. R., Gupta, S., Pichumani, K., Regan, L., and Stone, M. J. (2003) Covariation of backbone motion throughout a small protein domain, *Nat. Struct. Biol. 10*, 962−965.
8. Goehlert, V. A., Krupinska, E., Regan, L., and Stone, M. J. (2004) Analysis of side chain mobility among protein G B1 domain mutants with widely varying stabilities, *Protein Sci. 13*, 3322−3330.
9. de Lorimier, R., Hellinga, H. W., and Spicer, L. D. (1996) NMR studies of structure, hydrogen exchange, and main-chain dynamics in a disrupted-core mutant of thioredoxin, *Protein Sci. 5*, 2552−2565.

10. Mittermaier, A., and Kay, L. E. (2004) The response of internal dynamics to hydrophobic core mutations in the SH3 domain from the Fyn tyrosine kinase, *Protein Sci. 13*, 1088−1099.
11. Beeser, S. A., Goldenberg, D. P., and Oas, T. G. (1997) Enhanced protein flexibility caused by a destabilizing amino acid replacement in BPTI, *J. Mol. Biol. 269*, 154−164.
12. Hanson, W. M., Beeser, S. A., Oas, T. G., and Goldenberg, D. P. (2003) Identification of a residue critical for maintaining the functional conformation of BPTI, *J. Mol. Biol. 333*, 425−441.
13. Mulder, F. A. A., Hon, B., Muhandiram, D. R., Dahlquist, F. W., and Kay, L. E. (2000) Flexibility and ligand exchange in a buried cavity mutant of T4 lysozyme studied by multinuclear NMR, *Biochemistry 39*, 12614−12622.
14. Zhang, F., and Bruschweiler, R. (2002) Contact model for the prediction of NMR N−H order parameters in globular proteins, *J. Am. Chem. Soc. 124*, 12654−12655.
15. Minor, D. L., and Kim, P. S. (1996) Context-dependent secondary structure formation of a designed protein sequence, *Nature 380*, 730−734.
16. Seewald, M. J., Pichumani, K., Stowell, C., Tibbals, B. V., Regan, L., and Stone, M. J. (2000) The role of backbone conformational heat capacity in protein stability: Temperature-dependent dynamics of the B1 domain of *Streptococcal* protein G, *Protein Sci. 9*, 1177−1193.
17. Minor, D. L., and Kim, P. S. (1994) Measurement of the β-sheet-forming propensities of amino acids, *Nature 367*, 660−663.
18. Alexander, P., Fahnestock, S., Lee, T., Orban, J., and Bryan, P. (1992) Thermodynamic Analysis of the Folding of the Streptococcal Protein-G Igg-Binding Domains B1 and B2: Why Small Proteins Tend to Have High Denaturation Temperatures, *Biochemistry 31*, 3597−3603.
19. Kay, L. E., Torchia, D. A., and Bax, A. (1989) Backbone dynamics of proteins as studied by ^{15}N inverse detected heteronuclear NMR spectroscopy: Application to staphylococcal nuclease, *Biochemistry 28*, 8972−8979.
20. Farrow, N. A., Muhandiram, R., Singer, A. U., Pascal, S. M., Kay, C. M., Gish, G., Shoelson, S. E., Pawson, T., Forman-Kay, J. D., and Kay, L. E. (1994) Backbone dynamics of a free and phosphopeptide-complexed Src homology 2 domain studied by ^{15}N NMR relaxation, *Biochemistry 33*, 5984−6003.
21. Kroenke, C. D., Loria, J. P., Lee, L. K., Rance, M., and Palmer, A. G. (1998) Longitudinal and transverse ^{1}H-^{15}N dipolar ^{15}N chemical shift anisotropy relaxation interference: Unambiguous determination of rotational diffusion tensors and chemical exchange effects in biological macromolecules, *J. Am. Chem. Soc. 120*, 7905−7915.
22. Zhang, O. W., Kay, L. E., Olivier, J. P., and Forman-Kay, J. D. (1994) Backbone ^{1}H and ^{15}N resonance assignments of the N-terminal Sh3 domain of Drk in folded and unfolded states using enhanced-sensitivity pulsed-field gradient NMR techniques, *J. Biomol. NMR 4*, 845−858.
23. Fushman, D., and Cowburn, D. (1998) Model-independent analysis of ^{15}N chemical shift anisotropy from NMR relaxation data. Ubiquitin as a test example, *J. Am. Chem. Soc. 120*, 7109−7110.
24. Kuszewski, J., Gronenborn, A. M., and Clore, G. M. (1999) Improving the packing and accuracy of NMR structures with a pseudopotential for the radius of gyration, *J. Am. Chem. Soc. 121*, 2337−2338.
25. Bruschweiler, R., Liao, X. B., and Wright, P. E. (1995) Long-range motional restrictions in a multidomain zinc-finger protein from anisotropic tumbling, *Science 268*, 886−889.
26. Lipari, G., and Szabo, A. (1982) Model-free approach to the interpretation of nuclear magnetic resonance relaxation in macromolecules. 1. Theory and range of validity, *J. Am. Chem. Soc. 104*, 4546−4559.
27. Lipari, G., and Szabo, A. (1982) Model-free approach to the interpretation of nuclear magnetic resonance relaxation in macromolecules. 2. Analysis of experimental results, *J. Am. Chem. Soc. 104*, 4559−4570.
28. Clore, G. M., Driscoll, P. C., Wingfield, P. T., and Gronenborn, A. M. (1990) Analysis of the backbone dynamics of interleukin-1β using two-dimensional inverse detected heteronuclear ^{15}N−^{1}H NMR spectroscopy, *Biochemistry 29*, 7387−7401.
29. Clore, G. M., Szabo, A., Bax, A., Kay, L. E., Driscoll, P. C., and Gronenborn, A. M. (1990) Deviations from the simple 2-parameter model-free approach to the interpretation of ^{15}N nuclear magnetic-relaxation of proteins, *J. Am. Chem. Soc. 112*, 4989−4991.
30. Barbato, G., Ikura, M., Kay, L. E., Pastor, R. W., and Bax, A. (1992) Backbone dynamics of calmodulin studied by ^{15}N relaxation using inverse detected two-dimensional NMR spectroscopy: The central helix is flexible, *Biochemistry 31*, 5269−5278.
31. Mandel, A. M., Akke, M., and Palmer, A. G., III (1995) Backbone dynamics of *Escherichia coli* ribonuclease HI: Correlations with structure and function in an active enzyme, *J. Mol. Biol. 246*, 144−163.
32. Smith, C. K., Withka, J. M., and Regan, L. (1994) A thermodynamic scale for the β-sheet forming tendencies of the amino acids, *Biochemistry 33*, 5510−5517.
33. Schurr, J. M., Babcock, H. P., and Fujimoto, B. S. (1994) A test of the model-free formulas. Effects of anisotropic rotational diffusion and dimerization, *J. Magn. Reson., Ser. B 105*, 211−224.
34. Gronenborn, A. M., Filpula, D. R., Essig, N. Z., Achari, A., Whitlow, M., Wingfield, P. T., and Clore, G. M. (1991) A novel, highly stable fold of the immunoglobulin binding domain of streptococcal protein G, *Science 253*, 657−661.
35. Levitt, M. (1978) Conformational preferences of amino acids in globular proteins, *Biochemistry 17*, 4277−4285.
36. Hutchinson, E. G., and Thornton, J. M. (1994) A revised set of potentials for β-turn formation in proteins, *Protein Sci. 3*, 2207−2216.
37. Wilmot, C. M., and Thornton, J. M. (1990) β-Turns and their distortions: A proposed new nomenclature, *Protein Eng. 3*, 479−493.

BI0608919